IEEE Access
Multidisciplinary ⋮ Rapid Review ⋮ Open Access Journal

Received October 22, 2021, accepted November 22, 2021, date of publication November 25, 2021,
date of current version December 6, 2021.

Digital Object Identifier 10.1109/ACCESS.2021.3130676

A Hybrid a–φ Cell Method for Solving Eddy–Current Problems in 3–D Multiply–Connected Domains

FEDERICO MORO[1], (Member, IEEE), ARTEM NAPOV[2], AND LORENZO CODECASA[3], (Member, IEEE)

[1]Dipartimento di Ingegneria Industriale, Università degli Studi di Padova, 35131 Padova, Italy
[2]Service de Métrologie Nucléaire, Université Libre de Bruxelles, 1050 Brussels, Belgium
[3]Dipartimento di Elettronica, Informazione e Bioingegneria, Politecnico di Milano, 20133 Milano, Italy

Corresponding author: Federico Moro (federico.moro@unipd.it)

ABSTRACT A hybrid a–φ Cell Method formulation for solving eddy–current problems in 3–D multiply–connected regions is presented. By using the magnetic scalar potential the number of degrees of freedom in the exterior domain with respect to the A, V–A formulation, typically implemented in commercial software for electromagnetic design, can be almost halved. On the other hand, the use of the magnetic vector potential in the interior domain improves the flexibility with respect to T–Ω formulation, since both conductive and magnetic parts can be easily modeled. By using a Cell Method variant, based on an augmented dual grid for discretization, electric and magnetic variables can be consistently coupled at the interface between interior and exterior domain. Global basis functions needed for representing the magnetic field in the insulating region are obtained by using for the first time iterative solvers relying on auxiliary space preconditioner and aggregation–based algebraic multigrid, with linear optimal complexity. These represent highly–efficient alternatives to traditional computational topology algorithms based on the concept of thick cut. As a result, an indefinite symmetric matrix system, amenable to fast iterative solution, is obtained. Numerical tests show high accuracy and fast convergence of the a–φ method on test cases with complex topology. Computational cost for both matrix assembly and linear system solution is limited even for large problems. Comparisons show that the a–φ method provides better performance than existing methods such as A, V–A and h–φ.

INDEX TERMS Eddy current, finite element method, cell method, multiply connected, electromagnetic.

I. INTRODUCTION

The solution of eddy–current problems is still challenging if real–size engineering models are considered. Commercial software for electromagnetic simulations most often implements the A, V–A formulation, discretized by edge finite elements, which naturally leads to a large number of degrees of freedom (DOFs) [1]. This formulation involves, however, the solution of an ill–conditioned curl–curl system, hardly treated by state–of–the–art solvers. A possible solution is to reduce the number of DOFs by introducing a scalar potential such as the T–Ω method [2]. This solution strategy poses, however, some serious challenges when field problems with multiply connected domains are to be modeled. The use of potentials implies additional data structures, i.e. the so–called *thick cuts*, which are typically constructed by computational topology algorithms of high–complexity [3], [4].

A novel strategy, which allows for scalar potential in multiply connected domains without making thick cuts, has been recently proposed by the authors for the h–φ method in [5]. Global basis functions needed for representing the magnetic field in the insulating region are there obtained by using fast iterative solvers, greatly reducing computational complexity with respect to cut algorithms. However, complexity of such solvers is non–optimal, being super–linear with respect to the number of DOFs. Moreover, the h–φ formulation requires to restrict the use of $\mathbf{h}$ variables (i.e., mmfs along mesh edges) to conductive parts only. For instance, this limits the

The associate editor coordinating the review of this manuscript and approving it for publication was Wei E. I. Sha.

possibility of simplifying the topology of insulating domain where global basis functions are needed. On the contrary, the A, V–A method offers more flexibility, since the magnetic vector potential $\mathbf{A}$ can be used also in the insulating domain.

In order to lower the number of DOFs of the A, V–A formulation, while preserving its robustness and flexibility, hybrid formulations based on the Finite Element Method (FEM), mixing scalar and vector potentials, were proposed since the early 1980s [6]–[8]. The A–φ method makes use of $\mathbf{A}$ in the conductive domains and of the reduced magnetic scalar potential φ in the air domain, in presence of current–driven coils. The use of a total scalar potential ψ was also proposed in order to avoid cancellation errors inside high–permeable magnetic media [9]. First implementations were based, however, on the use of nodal shape functions for interpolating both φ and Cartesian components of $\mathbf{A}$. The unnatural enforcement of continuity brought from these functions led to an uneven behavior of fields in the vicinity of interfaces between different media. The same problem was observed at air/conductor interfaces also when modeling problems with multiply connected regions by using cuts [10]. To solve these issues the introduction of V variable in the conductive regions was proposed in [11]. In particular, to solve multiply connected problems, it was proposed in [12] to extend $\mathbf{A}$ region also to the non–conductive domain in order to make φ region simply–connected. A gauge technique, able to ensure the uniqueness of $\mathbf{A}$, was proposed in [13] in order to improve the convergence rate of the ICCG iterative solver.

The introduction of edge finite elements for interpolating $\mathbf{A}$, instead of nodal shape functions, made it possible to enforce across finite elements the continuity of tangent component only. In such a way, problems with inhomogeneous media were modeled without need of V, thus minimizing the number of DOFs [14]. One of the first edge–element implementations of the A–φ method was proposed by Kameari, who noticed that the mixed use of variables with different nature, i.e., the electric variable $\mathbf{A}$ (related to the electric field) and the magnetic variable φ (related to the magnetic field), led to some physical inconsistencies in the solution [15]. This issue was theoretically investigated by Bossavit in [16], who outlined how a consistent *hybrid formulation* (i.e., based on the use of both electric and magnetic variables) could be built only by using either Lagrange multipliers (to enforce field trace continuity at the interface between $\mathbf{A}$ and φ regions) or a boundary integral operator (to solve the field problem only in the $\mathbf{A}$ region by using the Dirichlet-to-Neumann map). The first approach has been only theoretically investigated in [17]. Conversely, a number of hybrid formulations based on the Boundary Element Method (BEM), discretizing a boundary integral operator, have been proposed (see, e.g., [18], [19]).

Hybrid methods, based on the definition of a boundary integral operator and formulated in terms of $\mathbf{A}$, φ variables, have been recently proposed for solving multiply–connected eddy–current problems [20], [21]. These formulations make it possible to avoid the air region meshing by combining the Cell Method (CM), for discretizing the interior domain with conductors, and the BEM, for the exterior domain. The CM discretization scheme is limited to first–order convergence like mimetic discretization schemes. The main drawback related to the BEM is that a dense block in the final matrix system is generated, typically involving high–computational costs in the case of large–size problems. It can be noted, however, that, by using the theoretical discretization framework presented in [21] for developing consistent hybrid formulations, an alternative coupling strategy for matching potentials at the interface can be designed.

In this work, a hybrid formulation relying on the CM discretization of both interior and exterior problems is presented. The key idea is that $\mathbf{A}$ and φ cannot be discretized in a compatible manner by using a standard finite element approach, based on a single mesh only. According to Tonti's classification of physical variables, a pair of dual cell complexes need to be used for a compatible discretization [22]. The main advantage of the a–φ method with respect to the h–φ method, already presented in [5], is that discrete field $\mathbf{a}$, i.e., line integrals of $\mathbf{A}$ along mesh edges, can be used also for the discretization of part of the non–conductive domain. Moreover, global basis functions needed for representing the magnetic field in the insulating region are obtained by a novel variant of the algorithm proposed in [20], which relies only on the iterative solution of equivalent magnetostatic matrix systems. In such a way, for the first time, iterative solvers with linear optimal computational complexity can be used.

The paper is organized as follows. The eddy–current problem in the continuous setting and topological constraints are first examined in Section II. The main features of the CM discretization framework presented in [21] are briefly recalled in Section III. The generation of global basis functions and source field, both based on the use of iterative solvers for magnetostatics, is discussed in Section IV. The CM discretization of the eddy–current problem is discussed in Section V, where details about the discretization of both interior problem (in terms of $\mathbf{a}$ edge variables) and the exterior problem (in terms of nodal scalar potentials $\boldsymbol{\varphi}$) are given. Numerical results are finally presented in Section VI.

II. EDDY–CURRENT PROBLEM

The computational domain Ω of the eddy–current problem is depicted in Fig. 1. It is assumed to be a simply–connected and bounded region of $\mathbb{R}^3$. The boundary of Ω is $\partial\Omega$, i.e. a bounding box enclosing all model parts. The *interior subdomain* $\Omega_i = \bigcup_{k=1}^{n} \Omega_i^{(k)}$ is defined as the union of n open bounded and possibly multiply-connected domains $\Omega_i^{(k)} \subseteq \Omega_i$, $k = 1 \dots n$, which include conductive and/or magnetic media. Its complement $\Omega_e = \Omega \setminus \overline{\Omega}_i$ denotes the *exterior subdomain*, where $\overline{\Omega}_i$ is the set closure of Ω_i. The exterior region, made of insulating media (e.g., air or magnetic materials), is possibly multiply-connected, and includes field sources in the subdomain $\Omega_0 \subseteq \Omega_e$. The source region is strictly embedded in the exterior region, so that $\partial\Omega_0 \cap \partial\Omega_e = \emptyset$. Differently from the h–φ method in [5], the insulating region can be split here between Ω_i and Ω_e.

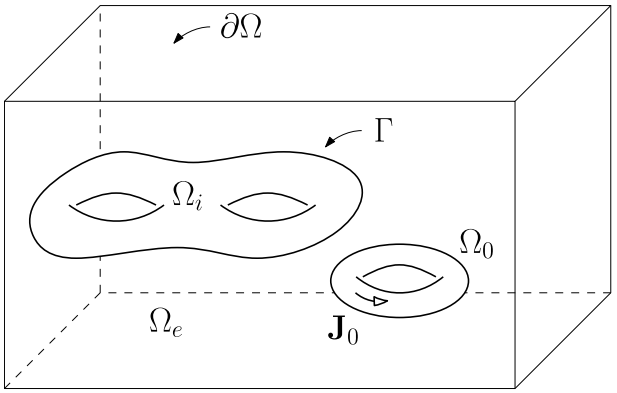

FIGURE 1. Computational domain Ω for the eddy current problem: Ω_i is the interior subdomain (with both magnetic and conductive parts), Ω_e is the exterior subdomain, and Ω_0 source domain with known current density $\mathbf{J_0}$; interface Γ separates Ω_i from Ω_e.

The boundaries of interior and exterior regions are indicated as $\partial\Omega_i$ and $\partial\Omega_e$, respectively. The *interface* between interior and exterior domains is the surface $\Gamma = \partial\Omega_i \cap \partial\Omega_e$, which can be partitioned into several connected components $\Gamma^{(k)} = \partial\Omega_i^{(k)}$, $k = 1, \ldots, n$. It is assumed that the interior region is strictly embedded in the computational domain, i.e., $\overline{\Omega_i} \subseteq \Omega$ with $\partial\Omega_i \cap \partial\Omega = \emptyset$. In such a way, it results $\Gamma = \partial\Omega_i$.

For developing the electromagnetic formulation it is useful to define the following outward unit normal vectors: $\mathbf{n}_{\partial\Omega_i}$ on $\partial\Omega_i$, $\mathbf{n}_{\partial\Omega_e}$ on $\partial\Omega_e$, and $\mathbf{n}_{\partial\Omega}$ on $\partial\Omega$. Note that $\mathbf{n}_{\partial\Omega_e} = \mathbf{n}_{\partial\Omega}$ on $\partial\Omega$. Moreover, $\mathbf{n}_{\partial\Omega_i} = -\mathbf{n}_{\partial\Omega_e}$ on Γ. Because $\Gamma = \partial\Omega_i$, the interface normal is defined as $\mathbf{n}_\Gamma = \mathbf{n}_{\partial\Omega_i}$. It is useful for discretizing interface conditions to define also the trace of $\partial\Omega_e$ on Γ, such that $\Gamma_e = \partial\Omega_e \cap \Gamma$, with normal $\mathbf{n}_{\Gamma_e} = -\mathbf{n}_\Gamma$.

In the eddy-current model, Maxwell's equations are taken in the low–frequency limit so that displacement currents are neglected. Magnetic field sources (i.e., AC current–driven coils at constant angular frequency ω) are represented by the source current density $\mathbf{J_0}$, which is a known solenoidal and time–harmonic field in Ω_0. By assuming linear conductive media (with piecewise constant electric conductivity σ) and magnetic media (with piecewise constant magnetic permeability μ), any time–harmonic scalar or vector field quantity in the time domain can be represented in the frequency domain as a phasor, i.e., complex–valued field. Under previous assumptions, the eddy–current model is governed by:

$$\nabla\times\mathbf{E} + \imath\,\omega\mathbf{B} = \mathbf{0}, \tag{1}$$
$$\nabla\times\mathbf{H} = \mathbf{J}, \tag{2}$$
$$\mathbf{J} = \sigma\mathbf{E} + \mathbf{J_0}, \tag{3}$$
$$\mathbf{H} = \nu\mathbf{B}, \tag{4}$$

where $\imath$ is the imaginary unit, $\nu = \mu^{-1}$ is the magnetic reluctivity, $\mathbf{E}$, $\mathbf{H}$ are the electric and magnetic field, respectively. Note that in practical applications (e.g., with stranded coils) Ω_0 can be assumed eddy–current free, i.e., with $\sigma = 0$. The magnetic flux density $\mathbf{B}$ and the current density $\mathbf{J}$ have to comply with the following conservation equations:

$$\nabla\cdot\mathbf{B} = 0, \tag{5}$$
$$\nabla\cdot\mathbf{J} = 0, \tag{6}$$

which are implicitly fulfilled by (1) and (2), respectively.

A. INTERIOR PROBLEM

Eddy currents are confined in the region Ω_i, which contains conductive and magnetic media. It is assumed that $\mathbf{J_0} = \mathbf{0}$ in (3), since source currents are only in Ω_0. The *interior field problem* is formulated in terms of $\mathbf{A}$, such that:

$$\mathbf{E} = -\imath\,\omega\mathbf{A}. \tag{7}$$

By letting (7) in (1), one obtains:

$$\mathbf{B} = \nabla\times\mathbf{A}, \tag{8}$$

which is equivalent to (5). By letting (3) and (4) in (2) and by using positions (7) and (8), the diffusion equation is obtained:

$$\nabla\times\,\nu\nabla\times\mathbf{A} + \imath\,\omega\,\sigma\,\mathbf{A} = \mathbf{0}. \tag{9}$$

B. EXTERIOR PROBLEM

The exterior region does not include any conductive part by definition; hence, eddy currents are not present there. By combining (2) and (3), with $\sigma = 0$, one obtains:

$$\nabla\times\mathbf{H} = \mathbf{J_0}. \tag{10}$$

The source field $\mathbf{H}_0$ is defined as any field in Ω_e such that $\nabla\times\mathbf{H}_0 = \mathbf{J}_0$. This means that the reduced magnetic field $\mathbf{H}_r = \mathbf{H} - \mathbf{H}_0$ is curl–free. Therefore, the corresponding cost $\mathbf{H}_r + B^1_{\mathrm{dR}}(\Omega_e)$, with $B^1_{\mathrm{dR}}(\Omega_e)$ space of gradients, is an element of the first de Rham cohomology group $H^1_{\mathrm{dR}}(\Omega_e)$. From de Rham theorem it follows that this group has finite dimension β_1, i.e., the first Betti number of Ω_e. This means that $\mathbf{H}_r$ (modulo gradient) can be expressed as a linear combination of *loop fields* $\mathbf{T}_k$, with $k = 1, \ldots, \beta_1$, which are the representatives of a basis of $H^1_{\mathrm{dR}}(\Omega_e)$. These vector fields are a basis of curl–free fields in Ω_e that are not gradient of any scalar field. The *first de Rham cohomology basis* is typically constructed by using computational topology algorithms with high–complexity (see, e.g., [23]). These are not adopted here because loop fields are built directly at the algebraic level. A variant of the algorithm in [5] is proposed in Section IV.

The *exterior field problem* in Ω_e is formulated in terms of scalar potential φ. As discussed in [5], this variable is different from the magnetic reduced scalar potential typically used in literature. To avoid the introduction of cuts the following decomposition of the magnetic field in Ω_e is adopted:

$$\mathbf{H} = \mathbf{H}_0 + \nabla\varphi + \sum_{k=1}^{\beta_1} \xi_k\,\mathbf{T}_k, \tag{11}$$

where ξ_k are complex coefficients, which are not necessarily circulations along loops as with thick cuts based expansions, and are determined at the solution stage, after discretization.

Topological constraints for enforcing ξ_k, $k = 1, \ldots, \beta_1$, are derived as follows. By applying the *virtual work principle* in Ω_e, the following orthogonality condition is obtained [20]:

$$\int_{\Omega_e} \mathbf{T}_k \cdot (\mathbf{B} - \nabla\times \mathbf{A})\, d\Omega = 0, \quad k = 1, \ldots, \beta_1. \quad (12)$$

Integrating by parts the second term and noting that $\mathbf{T}_k$ are curl–free fields in Ω_e, this becomes:

$$\int_{\Omega_e} \mathbf{T}_k \cdot \mathbf{B}\, d\Omega + \int_{\partial\Omega_e} \mathbf{T}_k \cdot \mathbf{A} \times \mathbf{n}_{\partial\Omega_e}\, d\Gamma = 0. \quad (13)$$

It has to be noted that the exterior domain boundary can be partitioned as $\partial\Omega_e = \Gamma_e \cup \partial\Omega$. By assuming a tangent magnetic flux density on the domain boundary, i.e., $\mathbf{A} \times \mathbf{n}_{\partial\Omega} = \mathbf{0}$ on $\partial\Omega$, last equation becomes for any $k = 1, \ldots, \beta_1$:

$$\int_{\Omega_e} \mathbf{T}_k \cdot \mathbf{B}\, d\Omega - \int_{\Gamma_e} \mathbf{A} \cdot \mathbf{T}_k \times \mathbf{n}_{\Gamma_e}\, d\Gamma = 0. \quad (14)$$

By noting that the exterior domain is made of insulating media, (4) can be expressed as:

$$\mathbf{B} = \mu\mathbf{H}. \quad (15)$$

By inserting (11) in (15) and by using (5), the following Poisson's equation for magnetostatics is obtained:

$$-\nabla\cdot \mu\, \nabla\varphi = \nabla\cdot \mu\mathbf{H}_0 + \sum_{k=1}^{\beta_1} \xi_k \nabla\cdot \mu\mathbf{T}_k. \quad (16)$$

The exterior problem is solved by assuming homogeneous Neumann BCs on $\partial\Omega$ and suitable interface conditions on Γ.

C. INTERFACE CONDITIONS

The interior and exterior problems are linked together by interface conditions, which state that the tangent component of the magnetic field and the normal component of the magnetic flux density have to be continuous across Γ. Dirichlet γ_D and Neumann γ_N *trace operators* are defined, as [24]:

$$\gamma_D\mathbf{A} = \mathbf{n}_\Gamma \times (\mathbf{A} \times \mathbf{n}_\Gamma), \quad (17)$$
$$\gamma_N\mathbf{A} = (\nabla\times \mathbf{A}) \times \mathbf{n}_\Gamma. \quad (18)$$

By denoting with $+$ the exterior traces (i.e., approaching Γ from outside along $\mathbf{n}_\Gamma$) and with $-$ the interior ones, the conservation of $\mathbf{B}$ normal component reads:

$$\gamma_D^-\mathbf{A} = \gamma_D^+\mathbf{A}, \quad (19)$$

where $\gamma_D^-\mathbf{A}$ is the Dirichlet condition for the interior problem. By assuming that magnetic materials are contained only in Ω_i, the conservation of $\mathbf{H}$ tangent component reads:

$$\nu^-\gamma_N^-\mathbf{A} = \nu^+\gamma_N^+\mathbf{A}, \quad (20)$$

where $\nu^\pm$ are the reluctivity values of materials sharing Γ.

III. CELL METHOD WITH AUGMENTED DUAL GRID

As it was noted by Bossavit in [16], electric and magnetic variables cannot be adopted in a variational FEM formulation at the same time. The main reason is that a unique chain complex, related to a single mesh and mimicking differential operators, is used within FEM discretization process [25]. A different discretization framework, illustrated in [21] and based on a pair of chain complexes, is here adopted.

A. COMPUTATIONAL GRIDS

The interior and exterior field problems are discretized into a set of linear equations by using a Cell Method variant based on the concept of *augmented dual grid* [26]. In such a way a combinatorial description of the field problem is provided, resulting in a network–like model. The main difference with the original CM formulation proposed by Tonti (see, e.g., [22], [27]) is that, for any domain Ω_k, the bulk dual grid $\widetilde{\mathcal{G}}_{\Omega_k}$ is augmented by its corresponding boundary dual grid $\widetilde{\mathcal{G}}_{\partial\Omega_k}$. This makes it possible to properly enforce both interface and boundary conditions. Dual grids are constructed by joining the centers of edges, faces, and volumes of the bulk primal grid $\mathcal{G}_{\Omega_k}$ (i.e., the tetrahedral mesh) and those of the boundary primal grid $\mathcal{G}_{\partial\Omega_k}$ (i.e., the restriction of $\mathcal{G}_{\Omega_k}$ to $\partial\Omega_k$). The union of the dual grid and of the boundary dual grid is the augmented dual grid $\widetilde{\mathcal{G}}_{\Omega_k\partial\Omega_k}$. A one–to–one correspondence is thus established between geometric entities of primal and dual grids. Details of this construction are given in [21].

Because of such one–to–one correspondence, geometric entities of $\widetilde{\mathcal{G}}_{\partial\Omega_k}$ and $\widetilde{\mathcal{G}}_{\Omega_k}$ inherit their outer orientations from those of $\mathcal{G}_{\partial\Omega_e}$ and $\mathcal{G}_{\Omega_e}$, with inner orientations.

B. DISCRETE FIELDS

Once orientation has been fixed, a physical quantity can be associated to the geometric entity with its own sign convention, likewise components in electric networks. For instance, any primal edge e can be oriented by its tangent vector $\mathbf{t}$, pointing from one end to the other (i.e., inner orientation), so that the electromotive force (emf) related to it becomes $\varepsilon_e = \int_e \mathbf{E}\cdot\mathbf{t}\, d\gamma$. Computing DOFs over the whole interior domain one obtains a column vector $\mathbf{e}_{\Omega_i} = (\varepsilon_e)_{e\in\mathcal{G}_{\Omega_i}}$. These arrays of DOFs are column vectors, hereafter indicated in lowercase bold notation. Other arrays defined in Ω_i are: line integrals of the magnetic vector potential along primal edges, i.e., $\mathbf{a}_{\Omega_i} = (a_e)_{e\in\mathcal{G}_{\Omega_i}}$, with $a_e = \int_e \mathbf{A}\cdot\mathbf{t}\, d\gamma$; magnetic fluxes through primal faces f, i.e., $\mathbf{b}_{\Omega_i} = (b_f)_{f\in\mathcal{G}_{\Omega_i}}$, where $b_f = \int_f \mathbf{B}\cdot\mathbf{n}\, d\sigma$ and $\mathbf{n}$ is the normal vector related to f; magnetomotive forces (mmfs) along dual edges $\widetilde{e}$, i.e., $\widetilde{\mathbf{h}}_{\Omega_i} = (\widetilde{h}_{\widetilde{e}})_{\widetilde{e}\in\widetilde{\mathcal{G}}_{\Omega_i}}$, with $\widetilde{h}_{\widetilde{e}} = \int_{\widetilde{e}} \mathbf{H}\cdot\mathbf{t}\, d\gamma$; currents through bulk dual faces $\widetilde{f}$, i.e., $\widetilde{\mathbf{j}}_{\Omega_i} = (\widetilde{j}_{\widetilde{f}})_{\widetilde{f}\in\widetilde{\mathcal{G}}_{\Omega_i}}$, with $\widetilde{j}_{\widetilde{f}} = \int_{\widetilde{f}} \mathbf{J}\cdot\mathbf{n}\, d\sigma$. In the exterior region main discrete fields are: scalar potentials at primal nodes n, i.e., $\boldsymbol{\varphi}_{\Omega_e} = (\varphi_n)_{n\in\mathcal{G}_{\Omega_e}}$; mmfs on primal edges $\mathbf{h}_{\Omega_e} = (h_e)_{e\in\mathcal{G}_{\Omega_e}}$; magnetic fluxes through dual faces $\widetilde{\mathbf{b}}_{\Omega_e} = (\widetilde{b}_{\widetilde{f}})_{\widetilde{f}\in\widetilde{\mathcal{G}}_{\Omega_e}}$. Similar definitions hold at interface grids, which take sign conventions from boundary grids of Ω_i,

e.g., reduced magnetic potentials at interface dual nodes $\widetilde{\boldsymbol{\varphi}}_\Gamma$ and mmfs along dual edges $\widetilde{\mathbf{h}}_\Gamma$.

C. DISCRETE OPERATORS

Discrete operators are obtained by applying Stokes' theorem to partial differential equations. For instance, from (8), the magnetic flux through any primal face becomes:

$$b_f = \int_f \nabla\times\mathbf{A}\cdot\mathbf{n}\,d\sigma = \int_{\partial f}\mathbf{A}\cdot\mathbf{t}d\gamma = \sum_{e\in\partial f} C_{f,e}\,a_e, \quad (21)$$

where $C_{f,e} = \pm 1$ is the face–to–edge incidence number ($+1$ if the orientation of the face boundary ∂f is consistent with that of the edge e) and a_e is the edge DOF defined above. On the whole primal grid of the interior region, (21) becomes:

$$\mathbf{b}_{\Omega_i} = \mathbf{C}_{\Omega_i}\,\mathbf{a}_{\Omega_i}, \quad (22)$$

where $\mathbf{C}_{\Omega_i} = (C_{f,e})_{f,e\in\mathcal{G}_{\Omega_i}}$ is the faces–to–edges incidence matrix of $\mathcal{G}_{\Omega_i}$. Other useful incidence matrices for the interior problem are: $\widetilde{\mathbf{C}}_{\Omega_i} = \mathbf{C}_{\Omega_i}^{\mathrm{T}}$ (faces–to–edges incidence matrix of $\widetilde{\mathcal{G}}_{\Omega_i}$), $\widetilde{\mathbf{C}}_{\Omega_i\Gamma}$ (faces of $\widetilde{\mathcal{G}}_{\Omega_i}$ to edges of $\widetilde{\mathcal{G}}_\Gamma$). For the exterior problem: $\mathbf{G}_{\Omega_e}$ (edges–to–nodes of $\mathcal{G}_{\Omega_e}$), $\widetilde{\mathbf{C}}_{\Omega_e\Gamma_e}$ (faces of $\widetilde{\mathcal{G}}_{\Omega_e}$ to edges of $\widetilde{\mathcal{G}}_{\Gamma_e}$), $\widetilde{\mathbf{D}}_{\Omega_e} = -\mathbf{G}_{\Omega_e}^{\mathrm{T}}$ (volumes–to–faces of $\widetilde{\mathcal{G}}_{\Omega_e}$), $\widetilde{\mathbf{D}}_{\Omega_e\Gamma_e}$ (volumes of $\widetilde{\mathcal{G}}_{\Omega_e}$ to faces of $\widetilde{\mathcal{G}}_{\Gamma_e}$). The definition of interface conditions requires $\mathbf{G}_\Gamma$ (edges–to–nodes of $\mathcal{G}_\Gamma$) and $\widetilde{\mathbf{C}}_\Gamma = -\mathbf{G}_\Gamma^{\mathrm{T}}$ (the faces–to–edges of $\widetilde{\mathcal{G}}_\Gamma$). Note that the last relationship is simply the restriction to the interface of the corresponding bulk property $\widetilde{\mathbf{D}}_{\Omega_e} = -\mathbf{G}_{\Omega_e}^{\mathrm{T}}$.

Discrete fields on the primal complex are mapped to those of the dual complex by using global constitutive relationships. In the interior region, by assuming $\mathbf{J}_0 = \mathbf{0}$, the local constitutive relationship for conductors (3) reads $\mathbf{J} = \sigma\mathbf{E}$. The electric field is locally interpolated by piecewise constant edge basis functions $\mathbf{w}_e$, defined in [28]. These are called also *edge elements* in the following. By using the construction based on the *energy approach* described in [21], one obtains the corresponding global relationship on Ω_i:

$$\widetilde{\mathbf{j}}_{\Omega_i} = \mathbf{M}_{\sigma,\Omega_i}\,\mathbf{e}_{\Omega_i}, \quad (23)$$

where the conductance matrix $\mathbf{M}_{\sigma,\Omega_i} = (m_{\sigma,ee'})_{e,e'\in\mathcal{G}_{\Omega_i}}$ of size $E_{\Omega_i}\times E_{\Omega_i}$ (E_{Ω_i} number of edges of $\mathcal{G}_{\Omega_i}$) is defined as:

$$m_{\sigma,ee'} = \int_{\Omega_i}\sigma\,\mathbf{w}_e\cdot\mathbf{w}_{e'}\,d\Omega. \quad (24)$$

Similarly, the magnetic flux density can be locally interpolated by using piecewise constant face functions $\mathbf{w}_f$, defined in [28]. These are called also *face elements* in the following. From the local magnetic constitutive relationship (4), one obtains the corresponding global relationship in Ω_i:

$$\widetilde{\mathbf{h}}_{\Omega_i} = \mathbf{M}_{\nu,\Omega_i}\,\mathbf{b}_{\Omega_i}, \quad (25)$$

where the reluctance matrix $\mathbf{M}_{\nu,\Omega_i} = (m_{\nu,ff'})_{f,f'\in\mathcal{G}_{\Omega_i}}$ of size $F_{\Omega_i}\times F_{\Omega_i}$ (F_{Ω_i} number of faces of $\mathcal{G}_{\Omega_i}$) is defined as:

$$m_{\nu,ff'} = \int_{\Omega_i}\nu\,\mathbf{w}_f\cdot\mathbf{w}_{f'}\,d\Omega. \quad (26)$$

According to the energy approach both constitutive matrices (24) and (26) are proven to be positive definite.

Both sets of basis functions $\mathbf{w}_e$ and $\mathbf{w}_f$ are locally defined on the primal grid, which is made of tetrahedrons. There is not a correspondent definition of basis functions for the dual grid, which is made of polyhedrons. For this reason, only discrete fields defined on the primal grid can be taken as problem unknowns, i.e., discrete potentials $\mathbf{a}_{\Omega_i}$ and $\boldsymbol{\varphi}_{\Omega_e}$.

Conversely, in the exterior domain, mmfs are mapped into magnetic fluxes by approximating the magnetic field in terms of edge elements. The global magnetic constitutive relationship in Ω_e is defined as:

$$\widetilde{\mathbf{b}}_{\Omega_e} = \mathbf{M}_{\mu,\Omega_e}\,\mathbf{h}_{\Omega_e}, \quad (27)$$

where the inductance matrix $\mathbf{M}_{\mu,\Omega_e} = (m_{\mu,ee'})_{e,e'\in\mathcal{G}_{\Omega_e}}$ of size $E_{\Omega_e}\times E_{\Omega_e}$ (E_{Ω_e} number of edges of $\mathcal{G}_{\Omega_e}$) is defined as (24), substituting μ with σ.

IV. TOPOLOGICAL FIELDS

From Stokes' theorem, by computing the line integral of (11) along any edge of $\mathcal{G}_{\Omega_e}$, the decomposition of the magnetic field in Ω_e at the discrete level becomes:

$$\mathbf{h}_{\Omega_e} = \mathbf{h}_{0,\Omega_e} + \mathbf{G}_{\Omega_e}\boldsymbol{\varphi}_{\Omega_e} + \mathbf{T}_{\Omega_e}\boldsymbol{\xi}_{\Omega_e}, \quad (28)$$

where $\mathbf{h}_{0,\Omega_e}$ is the array of source mmfs (corresponding to the line integrals of $\mathbf{H}_0$), and

$$\mathbf{T}_{\Omega_e} = \left[\mathbf{t}_{1,\Omega_e},\ldots,\mathbf{t}_{\beta_1,\Omega_e}\right], \quad (29)$$

$$\boldsymbol{\xi}_{\Omega_e} = \left[\xi_1,\ldots,\xi_{\beta_1}\right]^{\mathrm{T}}, \quad (30)$$

are the topological matrix and the array of coefficients in (11), respectively. Note that the kth column of the topological matrix $\mathbf{T}_{\Omega_e}$ is the array of DOFs related to the kth loop field, i.e., $\mathbf{t}_{k,\Omega_e} = (t_{k,e})_{e\in\mathcal{G}_{\Omega_e}}$, with $t_{k,e} = \int_e \mathbf{T}_k\cdot\mathbf{t}\,d\gamma$.

A. LOOP FIELDS

The topological matrix is computed by using a variant of the algorithm proposed in [5]. It is here shown that the use of Least Squares Minimal Residual (LSMR) or, equivalently, Least Squares with QR-factorization (LSQR) iterative solvers for rectangular systems can be avoided in favor of robust and efficient iterative solvers used in magnetostatics.

By applying Stokes' theorem to (10), for any primal face of $\mathcal{G}_{\Omega_e}$, one obtains the discrete form of Ampère law in Ω_e:

$$\mathbf{C}_{\Omega_e}\,\mathbf{h}_{\Omega_e} = \mathbf{j}_{0,\Omega_e}. \quad (31)$$

From (28) and (31), it can be deduced that $\mathbf{t}_{k,\Omega_e}$ are curl–free discrete fields, which are in the kernel of $\mathbf{C}_{\Omega_e}$. Therefore, the first step of the algorithm is to find any $\mathbf{u}_{\Omega_e}$ such that

$$\mathbf{C}_{\Omega_e}\mathbf{u}_{\Omega_e} = \mathbf{0}, \quad (32)$$

where a random entry of $\mathbf{u}_{\Omega_e}$, corresponding to an edge of $\mathcal{G}_\Gamma$, is set to one to get a non–trivial solution. In [5] the matrix system (32) is solved by using LSMR or LSQR. The following

equivalent square curl–curl system, typical of magnetostatic problems, is here considered instead:

$$\mathbf{C}_{\Omega_e}^{\mathrm{T}}\mathbf{M}_{\Omega_e}\mathbf{C}_{\Omega_e}\mathbf{u}_{\Omega_e} = \mathbf{0}, \tag{33}$$

where $\mathbf{M}_{\Omega_e}$ is any positive definite matrix of size $F_{\Omega_e} \times F_{\Omega_e}$, with F_{Ω_e} number of faces of $\mathcal{G}_{\Omega_e}$. The most convenient choice is to set $\mathbf{M}_{\Omega_e}$ equal to the identity matrix. Another option, although much more computationally expensive, is to define it as (26), by setting $\nu = 1$ as a fictitious reluctivity.

Theorem 1: Matrix system (32) *is equivalent to* (33).

Proof: If $\mathbf{u}_{\Omega_e}$ is a solution of (32), then it is also trivially a solution of (33). Vice versa, if $\mathbf{u}_{\Omega_e}$ is a solution of (33), then:

$$\mathbf{u}_{\Omega_e}^{\mathrm{T}}\mathbf{C}_{\Omega_e}^{\mathrm{T}}\mathbf{M}_{\Omega_e}\mathbf{C}_{\Omega_e}\mathbf{u}_{\Omega_e} = 0, \tag{34}$$

which implies (32), as $\mathbf{M}_{\Omega_e}$ is positive definite. □

The main advantage of solving (33) instead of (32) is that robust and efficient solvers for magnetostatics can be used.

Optimal (i.e., linear) complexity for the solution of (33) can be attained by means of an auxiliary space (AS) preconditioner (see, e.g., [29], [30]). The AS preconditioner involves the successive application of the symmetrized Gauss-Seidel iterative scheme, and an approximate solution of a few auxiliary matrix systems. The auxiliary systems are obtained by projection into discrete H^1 auxiliary spaces. In order to compute such solutions the block variant of AGMG solver is used [31]. The resulting AS preconditioner is used with a flexible variant of the preconditioned conjugate gradient (FPCG) method [32]. This strategy is verified by numerical experiments reported in Section VI.

A sub-optimal option, introducing only a small increase of computational complexity for problem sizes up to a few hundred thousands of DOFs, is to adopt PCG with symmetric successive over-relaxation (SSOR) preconditioner. Note that in [33] conjugate gradient is proven to converge for linear systems with positive semidefinite matrix as (33).

The orthogonal complement $\mathbf{v}_{\Omega_e} = \mathbf{u}_{\Omega_e} - \mathbf{G}_{\Omega_e}\boldsymbol{\varphi}_{\Omega_e}$ with respect to the space of gradients, i.e., the columns of $\mathbf{G}_{\Omega_e}$, is computed by solving a square symmetric matrix system:

$$\mathbf{G}_{\Omega_e}^{\mathrm{T}}\mathbf{M}_{\mu,\Omega_e}\mathbf{G}_{\Omega_e}\,\boldsymbol{\varphi}_{\Omega_e} = \mathbf{G}_{\Omega_e}^{\mathrm{T}}\mathbf{M}_{\mu,\Omega_e}\mathbf{u}_{\Omega_e}, \tag{35}$$

which can be treated very efficiently by an algebraic multigrid solver with linear time complexity such as AGMG [34].

Matrix systems (33) and (35) are solved for different random choices of the boundary condition, until the set of $\mathbf{v}_{\Omega_e}$ vectors defines a complete basis. A QR orthogonalization of such a set is used to determine the final loop field matrix (29).

From this construction it follows that loop fields are orthogonal to the columns of $\mathbf{G}_{\Omega_e}$, i.e.,

$$\mathbf{G}_{\Omega_e}^{\mathrm{T}}\mathbf{M}_{\mu,\Omega_e}\mathbf{T}_{\Omega_e} = \mathbf{0}. \tag{36}$$

This property, used several times in Section V, is key in the construction of the final matrix system of the hybrid method.

B. SOURCE MMFS

The array of source mmfs is obtained by assuming current–driven coils (i.e., $\mathbf{J}_0$ impressed in Ω_0) by using a variant of the procedure presented in [5]. Note that the source field $\mathbf{H}$, defined in Ω_e, does not have to be necessarily the solution of a magnetostatic problem, derived from Biot–Savart's integral.

In [5] the following rectangular matrix system is solved by LSMR or LSQR iterative solvers:

$$\mathbf{C}_{\Omega_e}\,\mathbf{h}_{0,\Omega_e} = \mathbf{j}_{0,\Omega_e}, \tag{37}$$

where $\mathbf{j}_{0,\Omega_e} = (j_{0,f})_{f\in\mathcal{G}_{\Omega_e}}$ is the array of source currents in Ω_e, with $j_{0,f} = \int_f \mathbf{J}_0 \cdot \mathbf{n}\, d\sigma$. The following equivalent square matrix system is here considered instead:

$$\mathbf{C}_{\Omega_e}^{\mathrm{T}}\mathbf{M}_{\Omega_e}\,\mathbf{C}_{\Omega_e}\,\mathbf{h}_{0,\Omega_e} = \mathbf{C}_{\Omega_e}^{\mathrm{T}}\mathbf{M}_{\Omega_e}\,\mathbf{j}_{0,\Omega_e}. \tag{38}$$

Note that, in order to solve (37) by an iterative solver, a curl–compatible RHS (i.e., lying in the range of $\mathbf{C}_{\Omega_e}$) has to be considered [35]. The following needs thus to be proven:

Theorem 2: $\mathbf{j}_{0,\Omega_e}$ *lies in the range of* $\mathbf{C}_{\Omega_e}$.

Proof: A procedure to obtain div–free source currents, i.e., such that $\mathbf{D}_{\Omega_0}\mathbf{j}_{\Omega_0} = \mathbf{0}$, is proposed in [5]. $\mathbf{j}_{0,\Omega_0}$ can be extended to the whole computational domain (which is simply–connected) by putting null entries for faces of $\mathcal{G}_{\Omega_e\setminus\Omega_0}$. Therefore, it follows also $\mathbf{D}_{\Omega}\,\mathbf{j}_{0,\Omega} = \mathbf{0}$. From $\beta_2 = 0$ (2^{nd} ord. Betti number), for a simply–connected domain, there it holds $\ker(\mathbf{D}_{\Omega}) = \mathrm{im}(\mathbf{C}_{\Omega})$ or, equivalently, $\mathbf{j}_{0,\Omega} \in \mathrm{im}(\mathbf{C}_{\Omega})$. This condition implies that there exists $\mathbf{h}_{0,\Omega}$ such that:

$$\mathbf{C}_{\Omega}\,\mathbf{h}_{0,\Omega} = \mathbf{j}_{0,\Omega}. \tag{39}$$

It can be observed now that $\mathbf{C}_{\Omega_e}$ shares the same coefficients of $\mathbf{C}_{\Omega}$ over the primal grid $\mathcal{G}_{\Omega_e}$, since any face of $\mathcal{G}_{\Omega_e}$ is incident to edges pertaining to $\mathcal{G}_{\Omega_e}$ itself only. Therefore, from (39), it follows that the restriction of $\mathbf{h}_{0,\Omega}$ to $\mathcal{G}_{\Omega_e}$ fulfills (37) or, equivalently, $\mathbf{j}_{0,\Omega_e} \in \mathrm{im}\left(\mathbf{C}_{\Omega_e}\right)$. □

With the last result the following can be proven:

Theorem 3: Matrix system (37) *is equivalent to* (38).

Proof: From Theorem 2 there exists $\mathbf{t}_{0,\Omega_e}$ such that $\mathbf{j}_{0,\Omega_e} = \mathbf{C}_{\Omega_e}\mathbf{t}_{0,\Omega_e}$. By substituting this expression at the RHS of both (37) and (38), and by posing $\mathbf{u}_{0,\Omega_e} = \mathbf{h}_{0,\Omega_e} - \mathbf{t}_{0,\Omega_e}$, it results:

$$\mathbf{C}_{\Omega_e}\mathbf{u}_{0,\Omega_e} = \mathbf{0}, \tag{40}$$

$$\mathbf{C}_{\Omega_e}^{\mathrm{T}}\mathbf{M}_{\Omega_e}\mathbf{C}_{\Omega_e}\mathbf{u}_{0,\Omega_e} = \mathbf{0}, \tag{41}$$

which, from Theorem 1, are proven to be equivalent. □

V. CELL METHOD FORMULATION

The CM is applied for discretizing both interior and exterior problems, defined in Section II in the continuous setting. The interior problem is formulated in terms of magnetic vector potential line integrals $\mathbf{a}_{\Omega_i}$, whereas the exterior problem is formulated in terms of scalar potentials $\boldsymbol{\varphi}_{\Omega_e}$ and $\boldsymbol{\xi}_{\Omega_e}$. Note that both sets of variables are defined on the primal grid, where edge and face functions—used for determining global constitutive relationships—are naturally defined.

A. INTERIOR PROBLEM

The construction of the discrete diffusion equation in Ω_i is like that of CM–BEM hybrid formulations [20], [21].

From Stokes' theorem applied to (2), by computing fluxes through dual faces of $\widetilde{\mathcal{G}}_{\Omega_i}$, the discrete Ampère law in Ω_i is:

$$\widetilde{\mathbf{C}}_{\Omega_i}\widetilde{\mathbf{h}}_{\Omega_i} + \widetilde{\mathbf{C}}_{\Omega_i\Gamma}\widetilde{\mathbf{h}}_{\Gamma} = \widetilde{\mathbf{j}}_{\Omega_i}. \tag{42}$$

The surface curl matrix $\widetilde{\mathbf{C}}_{\Omega_i\Gamma}$, introduced in [26], is needed in order to complete circulations of the magnetic field along the boundary of dual faces which are in one–to–one correspondence with primal edges of $\mathcal{G}_\Gamma$. $\widetilde{\mathbf{C}}_{\Omega_i\Gamma}$ can be built as the transpose of the selection matrix (with {0, 1} coefficients), which extracts the primal edges of $\mathcal{G}_\Gamma$ from those of $\mathcal{G}_{\Omega_i}$. The array of interface mmfs $\widetilde{\mathbf{h}}_\Gamma$ (related to dual edges of $\widetilde{\mathcal{G}}_\Gamma$) makes it possible to couple interior and exterior problems, through the definition of suitable interface conditions.

On the boundary of the interior domain, i.e., at the interface Γ, (42) corresponds to:

$$\widetilde{\mathbf{C}}_{\Gamma}\widetilde{\mathbf{h}}_{\Gamma} = \widetilde{\mathbf{j}}_{\Gamma}, \tag{43}$$

where $\widetilde{\mathbf{j}}_\Gamma = \mathbf{0}$, since no current flows out from Ω_i. By assembling (42) and (43) the Ampère law on the augmented dual grid, with the curl operator defined in [21], is obtained.

By inserting constitutive relationships (23) and (25) in (42), with $\widetilde{\mathbf{C}}_{\Omega_i} = \mathbf{C}_{\Omega_i}^{\mathrm{T}}$, the diffusion equation reads:

$$\mathbf{C}_{\Omega_i}^{\mathrm{T}}\mathbf{M}_{\nu,\Omega_i}\mathbf{b}_{\Omega_i} + \widetilde{\mathbf{C}}_{\Omega_i\Gamma}\widetilde{\mathbf{h}}_{\Gamma} = \mathbf{M}_{\sigma,\Omega_i}\mathbf{e}_{\Omega_i}. \tag{44}$$

By using flux conservation (22) and the discrete form of (7):

$$\mathbf{e}_{\Omega_i} = -\imath\,\omega\,\mathbf{a}_{\Omega_i}, \tag{45}$$

the diffusion equation finally becomes:

$$\left(\mathbf{C}_{\Omega_i}^{\mathrm{T}}\mathbf{M}_{\nu,\Omega_i}\mathbf{C}_{\Omega_i} + \imath\,\omega\,\mathbf{M}_{\sigma,\Omega_i}\right)\mathbf{a}_{\Omega_i} + \widetilde{\mathbf{C}}_{\Omega_i\Gamma}\widetilde{\mathbf{h}}_{\Gamma} = \mathbf{0}, \tag{46}$$

where the RHS is null since source currents are assumed to be confined in the region Ω_0, outside the exterior domain.

B. EXTERIOR PROBLEM

From the divergence theorem applied to (5), by computing magnetic fluxes through dual faces of $\widetilde{\mathcal{G}}_{\Omega_e}$, the discrete form of local Gauss's law in Ω_e is obtained:

$$\widetilde{\mathbf{D}}_{\Omega_e}\widetilde{\mathbf{b}}_{\Omega_e} + \widetilde{\mathbf{D}}_{\Omega_e\Gamma_e}\widetilde{\mathbf{b}}_{\Gamma_e} = \mathbf{0}, \tag{47}$$

where magnetic fluxes $\widetilde{\mathbf{b}}_{\Gamma_e}$ through dual faces of $\widetilde{\mathcal{G}}_{\Gamma_e}$ are computed with respect to the exterior normal $\mathbf{n}_{\partial\Omega_e}$, which is opposite to $\mathbf{n}_\Gamma$ on Γ. Note also that, because a tangent magnetic flux density is assumed on $\partial\Omega$, only interface fluxes are considered in the balance equation (47). Inserting (27) in (47), with $\widetilde{\mathbf{D}}_{\Omega_e} = -\mathbf{G}_{\Omega_e}^{\mathrm{T}}$, yields:

$$\mathbf{G}_{\Omega_e}^{\mathrm{T}}\,\mathbf{M}_{\mu,\Omega_e}\mathbf{h}_{\Omega_e} - \widetilde{\mathbf{D}}_{\Omega_e\Gamma_e}\widetilde{\mathbf{b}}_{\Gamma_e} = \mathbf{0}. \tag{48}$$

By letting (28) in (48) and exploiting the orthogonality relationship (36), the discrete form of local Gauss's law yields:

$$\mathbf{G}_{\Omega_e}^{\mathrm{T}}\mathbf{M}_{\mu,\Omega_e}\mathbf{G}_{\Omega_e}\boldsymbol{\varphi}_{\Omega_e} - \widetilde{\mathbf{D}}_{\Omega_e\Gamma_e}\widetilde{\mathbf{b}}_{\Gamma_e} = -\mathbf{G}_{\Omega_e}^{\mathrm{T}}\mathbf{M}_{\mu,\Omega_e}\mathbf{h}_{0,\Omega_e}. \tag{49}$$

Topological constraints necessary to enforce coefficients $\boldsymbol{\xi}_{\Omega_e}$ are obtained from the discretization of (14). Loop fields $\mathbf{T}_k$ are locally reconstructed in terms of edge basis functions. The first term in (14), for any $k = 1, \ldots, \beta_1$, thus becomes:

$$\int_{\Omega_e}\mathbf{T}_k\cdot\mathbf{B}\,d\Omega = \sum_{e=1}^{E_{\Omega_e}} t_{k,e}\int_{\Omega_e}\mathbf{w}_e\cdot\mathbf{B}\,d\Omega. \tag{50}$$

By assuming a locally constant magnetic flux density in each primal cell, i.e., tetrahedron of the mesh, the so–called *consistency property* of edge elements holds, i.e., any magnetic flux through the dual face $\widetilde{f}$ of $\widetilde{\mathcal{G}}_{\Omega_e}$ can be obtained as:

$$\widetilde{b}_{\widetilde{f}} = \int_{\Omega_e}\mathbf{w}_e\cdot\mathbf{B}\,d\Omega, \tag{51}$$

where the primal edge e of $\mathcal{G}_{\Omega_e}$ is one–to–one correspondence with $\widetilde{f}$. Therefore, (50) can be rewritten as:

$$\int_{\Omega_e}\mathbf{T}_k\cdot\mathbf{B}\,d\Omega = \sum_{e=1}^{E_{\Omega_e}} t_{k,e}\,\widetilde{b}_e = \mathbf{t}_{k,\Omega_e}^{\mathrm{T}}\widetilde{\mathbf{b}}_{\Omega_e}. \tag{52}$$

The second term in (14) can be approximated again by expressing the kth loop field in terms of edge elements, as:

$$\int_{\Gamma_e}\mathbf{A}\cdot\mathbf{T}_k\times\mathbf{n}_{\Gamma_e}\,d\Gamma = \sum_{e=1}^{E_{\Omega_e}} t_{k,e}\int_{\Gamma_e}\mathbf{A}\cdot\mathbf{w}_e\times\mathbf{n}_{\Gamma_e}\,d\Gamma, \tag{53}$$

where E_{Γ_e} is the number of primal edges of $\mathcal{G}_{\Gamma_e}$. Twisted edge elements $\mathbf{n}_{\Gamma_e}\times\mathbf{w}_e$, defined on the surface Γ_e, enjoy the consistency property as well, i.e., any line integral of $\mathbf{A}$ along the dual edge $\widetilde{e}$ of $\widetilde{\mathcal{G}}_\Gamma$ can be obtained as:

$$\widetilde{a}_e = -\int_{\Gamma_e}\mathbf{A}\cdot\mathbf{w}_e\times\mathbf{n}_{\Gamma_e}\,d\Gamma, \tag{54}$$

where the primal edge e of $\mathcal{G}_\Gamma$ is in one–to–one correspondence with $\widetilde{e}$. Therefore, (54) can be rewritten as:

$$\int_{\Gamma_e}\mathbf{A}\cdot\mathbf{T}_k\times\mathbf{n}_{\Gamma_e}\,d\Gamma = -\sum_{e=1}^{E_{\Gamma_e}} t_{k,e}\widetilde{a}_e = -\mathbf{t}_{k,\Gamma_e}^{\mathrm{T}}\widetilde{\mathbf{a}}_{\Gamma_e}. \tag{55}$$

By combining (52) and (55), topological constraints in the continuous setting (14) can be finally approximated as:

$$\mathbf{t}_{k,\Omega_e}^{\mathrm{T}}\widetilde{\mathbf{b}}_{\Omega_e} + \mathbf{t}_{k,\Gamma_e}^{\mathrm{T}}\widetilde{\mathbf{a}}_{\Gamma_e} = 0, \quad k = 1, \ldots, \beta_1. \tag{56}$$

Boundary DOFs can be extracted from bulk ones by noting that the transpose of an incidence matrix $\mathbf{C}_{\Omega_e\Gamma_e}$, defined on the augmented dual grid, is a selection matrix made of 0, 1 coefficients, such that $\mathbf{t}_{k,\Gamma_e} = \widetilde{\mathbf{C}}_{\Omega_e\Gamma_e}^{\mathrm{T}}\mathbf{t}_{k,\Omega_k}$. Therefore, by assembling discrete topological constraints, one obtains:

$$\mathbf{T}_{\Omega_e}^{\mathrm{T}}\widetilde{\mathbf{b}}_{\Omega_e} + \mathbf{T}_{\Omega_e}^{\mathrm{T}}\widetilde{\mathbf{C}}_{\Omega_e\Gamma_e}\widetilde{\mathbf{a}}_{\Gamma_e} = 0. \tag{57}$$

Magnetic fluxes from (47) can be eliminated as above by using (27) and (28). By using the transpose of the orthogonality relationship (36), (57) becomes:

$$\mathbf{T}_{\Omega_e}^{\mathrm{T}}\left[\mathbf{M}_{\mu,\Omega_e}\mathbf{T}_{\Omega_e}\boldsymbol{\xi}_{\Omega_e} + \widetilde{\mathbf{C}}_{\Omega_e\Gamma_e}\widetilde{\mathbf{a}}_{\Gamma_e}\right] = -\mathbf{T}_{\Omega_e}^{\mathrm{T}}\mathbf{M}_{\mu,\Omega_e}\mathbf{h}_{0,\Omega_e}. \tag{58}$$

C. INTERFACE CONDITIONS

The interior and exterior field problems are coupled together by enforcing the continuity of the magnetic flux through any face of $\mathcal{G}_\Gamma$, which corresponds to (19) in the continuous setting, and the continuity of the mmf through any edge of $\widetilde{\mathcal{G}}_\Gamma$, which corresponds to (20) in the continuous setting.

The magnetic flux continuity is a consequence of the continuity of line integrals of $\mathbf{A}$ across Γ. In fact, from (17) it can be deduced that $\mathbf{A} \times \mathbf{n}_\Gamma$ is continuous across Γ. By using this property and by letting $\mathbf{n}_\Gamma = -\mathbf{n}_{\Gamma_e}$ in (54), one obtains:

$$\widetilde{\mathbf{a}}_{\Gamma_e} = -\widetilde{\mathbf{a}}_\Gamma. \tag{59}$$

On the other hand, from (18), $\mathbf{H} \times \mathbf{n}_\Gamma$ is continuous across Γ. Therefore, by using a similar argument as above, it results:

$$\widetilde{\mathbf{h}}_\Gamma = -\widetilde{\mathbf{h}}_{\Gamma_e}, \tag{60}$$

where $\mathbf{h}_{\Omega_e}$ is defined by (28).

The DOFs defined on dual edges can be expressed in terms of those defined on primal edges by using a projection matrix $\mathbf{P}_\Gamma = (p_{ee'})_{e,e' \in \mathcal{G}_\Gamma}$, which is constructed as follows. By noting that $\mathbf{A}$ can be expanded in terms of edge elements and the consistency property holds over the interface, one obtains:

$$\widetilde{a}_e = -\int_\Gamma \mathbf{A} \cdot \mathbf{w}_e \times \mathbf{n}_\Gamma \, d\Gamma = \sum_{e'=1}^{E_\Gamma} p_{ee'} \, a_{e'}, \tag{61}$$

where:

$$p_{ee'} = \int_\Gamma \mathbf{w}_e \times \mathbf{w}_{e'} \cdot \mathbf{n}_\Gamma \, d\Gamma, \tag{62}$$

and $E_\Gamma = E_{\Gamma_e}$ is the number of interface primal edges. The primal–to–dual map (61) written in matrix form becomes:

$$\widetilde{\mathbf{a}}_\Gamma = \mathbf{P}_\Gamma \, \mathbf{a}_\Gamma. \tag{63}$$

From (62) the projection map results to be skew–symmetric, i.e., $\mathbf{P}_\Gamma^{\mathrm{T}} = -\mathbf{P}_\Gamma$. DOFs related to interface primal edges can be extracted from those related to interior edges by considering the transpose of the surface curl matrix in (42), i.e., $\mathbf{a}_\Gamma = \widetilde{\mathbf{C}}_{\Omega_i \Gamma_i}^{\mathrm{T}} \mathbf{a}_{\Omega_i}$. By letting (63) in (59), one obtains:

$$\widetilde{\mathbf{a}}_{\Gamma_e} = \mathbf{P}_\Gamma^{\mathrm{T}} \, \widetilde{\mathbf{C}}_{\Omega_i \Gamma}^{\mathrm{T}} \, \mathbf{a}_{\Omega_i}. \tag{64}$$

By applying $\mathbf{C}_\Gamma$ to both members of (64), the magnetic flux conservation across Γ can be finally deduced as:

$$\widetilde{\mathbf{b}}_{\Gamma_e} = \widetilde{\mathbf{C}}_\Gamma \, \mathbf{P}_\Gamma^{\mathrm{T}} \, \widetilde{\mathbf{C}}_{\Omega_i \Gamma}^{\mathrm{T}} \, \mathbf{a}_{\Omega_i}. \tag{65}$$

In a similar way, (60) becomes:

$$\widetilde{\mathbf{h}}_\Gamma = \mathbf{P}_\Gamma^{\mathrm{T}} \, \widetilde{\mathbf{C}}_{\Omega_e \Gamma_e}^{\mathrm{T}} \mathbf{h}_{\Omega_e}. \tag{66}$$

Note that (43) is implicitly fulfilled by (66), since all the components of $\mathbf{h}_{\Omega_e}$, i.e., source field, loop fields, and gradients, are curl-free on $\partial\Omega_e$.

D. COUPLED MATRIX SYSTEM

With the a–φ method, the final matrix system is directly formulated in terms of primal variables, defined on the tetrahedral mesh, namely potentials $\mathbf{a}_{\Omega_i}$, $\boldsymbol{\varphi}_{\Omega_e}$ and $\boldsymbol{\xi}_{\Omega_e}$. Therefore, the construction of the final system results to be easier than that of the h–φ method, in which Lagrange multipliers, defined on the dual edges of Γ, need to be eliminated before solution. The final system has the following block structure:

$$\begin{pmatrix} \mathbf{K}_{11} & \mathbf{K}_{12} & \mathbf{K}_{13} \\ \mathbf{K}_{21} & \mathbf{K}_{22} & \mathbf{O} \\ \mathbf{K}_{31} & \mathbf{O} & \mathbf{K}_{33} \end{pmatrix} \begin{pmatrix} \mathbf{a}_{\Omega_i} \\ \boldsymbol{\varphi}_{\Omega_e} \\ \boldsymbol{\xi}_{\Omega_e} \end{pmatrix} = \begin{pmatrix} \mathbf{f}_1 \\ \mathbf{f}_2 \\ \mathbf{f}_3 \end{pmatrix}. \tag{67}$$

This is constructed, row by row, as follows. The diffusion equation in Ω_i can be expressed in terms of potentials by letting (66) in (46). The following matrices are thus obtained:

$$\mathbf{K}_{11} = \mathbf{C}_{\Omega_i}^{\mathrm{T}} \mathbf{M}_{\nu,\Omega_i} \mathbf{C}_{\Omega_i} + \imath \, \omega \, \mathbf{M}_{\sigma,\Omega_i}, \tag{68}$$

$$\mathbf{K}_{12} = \widetilde{\mathbf{C}}_{\Omega_i \Gamma} \mathbf{P}_\Gamma^{\mathrm{T}} \widetilde{\mathbf{C}}_{\Omega_e \Gamma_e}^{\mathrm{T}} \mathbf{G}_{\Omega_e}, \tag{69}$$

$$\mathbf{K}_{13} = \widetilde{\mathbf{C}}_{\Omega_i \Gamma} \mathbf{P}_\Gamma^{\mathrm{T}} \widetilde{\mathbf{C}}_{\Omega_e \Gamma_e}^{\mathrm{T}} \mathbf{T}_{\Omega_e}. \tag{70}$$

The following column vector is obtained at RHS from (46):

$$\mathbf{f}_1 = -\widetilde{\mathbf{C}}_{\Omega_i \Gamma} \mathbf{P}_\Gamma^{\mathrm{T}} \widetilde{\mathbf{C}}_{\Omega_e \Gamma_e}^{\mathrm{T}} \mathbf{h}_{0,\Omega_e}. \tag{71}$$

The magnetic flux conservation for Ω_e can be expressed in terms of potentials by letting (65) in (49), yielding:

$$\mathbf{K}_{22} = -\mathbf{G}_{\Omega_e}^{\mathrm{T}} \mathbf{M}_{\mu,\Omega_e} \mathbf{G}_{\Omega_e}, \tag{72}$$

$$\mathbf{K}_{21} = \widetilde{\mathbf{D}}_{\Omega_e \Gamma_e} \widetilde{\mathbf{C}}_\Gamma \, \mathbf{P}_\Gamma^{\mathrm{T}} \, \widetilde{\mathbf{C}}_{\Omega_i \Gamma}^{\mathrm{T}}, \tag{73}$$

$$\mathbf{f}_2 = \mathbf{G}_{\Omega_e}^{\mathrm{T}} \mathbf{M}_{\mu,\Omega_e} \mathbf{h}_{0,\Omega_e}. \tag{74}$$

Note that $\mathbf{K}_{21} = \mathbf{K}_{12}^{\mathrm{T}}$ since $\widetilde{\mathbf{C}}_\Gamma = -\mathbf{G}_\Gamma^{\mathrm{T}}$ and the following property regarding selection matrices holds:

$$\mathbf{G}_\Gamma \, \widetilde{\mathbf{D}}_{\Omega_e \Gamma_e}^{\mathrm{T}} = \widetilde{\mathbf{C}}_{\Omega_e \Gamma_e}^{\mathrm{T}} \, \mathbf{G}_{\Omega_e}, \tag{75}$$

where $\widetilde{\mathbf{D}}_{\Omega_e \Gamma_e}^{\mathrm{T}}$ selects the primal nodes of $\mathcal{G}_\Gamma$ from $\mathcal{G}_{\Omega_e}$, and $\widetilde{\mathbf{C}}_{\Omega_e \Gamma_e}^{\mathrm{T}}$ selects the primal edges of $\mathcal{G}_\Gamma$ from those of $\mathcal{G}_{\Omega_e}$.

Finally, topological constraints provide the last row of the system, which is obtained by letting (64) in (58). It ensues:

$$\mathbf{K}_{31} = -\mathbf{T}_{\Omega_e}^{\mathrm{T}} \widetilde{\mathbf{C}}_{\Omega_e \Gamma_e} \mathbf{P}_\Gamma^{\mathrm{T}} \widetilde{\mathbf{C}}_{\Omega_i \Gamma}^{\mathrm{T}}, \tag{76}$$

$$\mathbf{K}_{33} = -\mathbf{T}_{\Omega_e}^{\mathrm{T}} \mathbf{M}_{\mu,\Omega_e} \mathbf{T}_{\Omega_e}, \tag{77}$$

$$\mathbf{f}_3 = \mathbf{T}_{\Omega_e}^{\mathrm{T}} \mathbf{M}_{\mu,\Omega_e} \mathbf{h}_{0,\Omega_e}, \tag{78}$$

where $\mathbf{K}_{31} = \mathbf{K}_{13}^{\mathrm{T}}$ because $\mathbf{P}_\Gamma$ is skew–symmetric.

The final matrix system (67) is symmetric indefinite and complex, therefore it is amenable to iterative solution by Transpose Free Quasi-Minimal Residual (TFQMR) solver, with the main advantage of low–memory requirements. In order to accelerate TFQMR convergence, SSOR preconditioner is applied to the following matrix system, equivalent to (67):

$$\mathbf{P}^{\mathrm{T}} \mathbf{K} \mathbf{P} \, \mathbf{x} = \mathbf{P}^{\mathrm{T}} \mathbf{f}, \tag{79}$$

where the projection matrix is defined as:

$$\mathbf{P} = \begin{bmatrix} \mathbf{1}_{E_{\Omega_i}} & \mathbf{G}_{\Omega_i} & \mathbf{0} \\ \mathbf{0} & \mathbf{1}_{N_{\Omega_I}} & \mathbf{0} \\ \mathbf{0} & \mathbf{0} & \mathbf{1}_{\beta_1} \end{bmatrix}, \tag{80}$$

where $\mathbf{1}_{E_{\Omega_i}}$, $\mathbf{1}_{N_{\Omega_I}}$, and $\mathbf{1}_{\beta_1}$ are identity matrices of size E_{Ω_i}, N_{Ω_I} (i.e., the number of primal nodes of $\mathcal{G}_{\Omega_i}$), and β_1, respectively. Numerical experiments in Section VI show that TFQMR + SSOR has a good performance if applied to (79).

VI. NUMERICAL RESULTS

The a–φ method is implemented in a vectorized MATLAB® code and tested on benchmarks presented in [21], namely the axisymmetric inductor and the Bath plate. The first test, with axisymmetric geometry, is used to get highly–accurate values from third–order 2–D FEM for convergence analyses. The second test is useful to assess the performance of a–φ method on a realistic 3–D eddy current problem. All numerical tests are run on a laptop with an Intel Core i7-6920HQ processor (2.9 GHz clock frequency) and 16 GB RAM, excepts those for Fig. 3, which are carried out on a desktop with Intel Xeon E5-2620 processor at 2.10GHz with 128 GB RAM.

A. AXISYMMETRIC INDUCTOR

Fig. 2 shows a sketch of the axisymmetric inductor (radial section), which consists in a cylindrical shell excited by an AC current–driven coil. The inductor core Ω_1 (5 mm inner radius, 10 mm outer radius, 40 mm long) is multiply–connected, with two symmetric holes (2 mm side, centered at $r = 7.5$ mm, $z = \pm 30$ mm), and it is made of conductive material (25 MS/m conductivity, 2 relative permeability). The inductor coil Ω_0 (square cross section, 4 mm side, centered at $r = 15$ mm, $z = 0$) carries 16 A at 200 Hz frequency. The air region is partitioned into Ω_2 subdomain (with holes) and Ω_3 subdomain (which includes Ω_0). The computational domain Ω is a cylinder (30 mm radius, 80 mm long).

A variant of the benchmark proposed in [5] is here considered, with the following modeling scenarios:

1) $\Omega_i = \Omega_1$ and $\Omega_e = \Omega_2 \cup \Omega_3$, i.e., the interior region is restricted to the core only and is multiply connected;
2) $\Omega_i = \Omega_1 \cup \Omega_2$ and $\Omega_e = \Omega_3$, i.e., the interior region is a cylinder (10 mm radius) which is simply connected and includes the core and part of the air domain.

Magnetic vector potential is defined in Ω_i, whereas the scalar potential is defined in Ω_e. For case 1, the exterior region is multiply connected (with $\beta_1 = 3$) so that three loop fields are expected to be generated by the algorithm in Section IV. For case 2, no loop fields are generated since Ω_e is simply connected (with $\beta_1 = 0$). The last scenario is useful to prove the accuracy of the a–φ method when model topology is simplified by extending the magnetic vector potential domain to the air region. Note that this cannot be realized with the h–φ method, not coupling electric and magnetic variables [5].

The magnetic field distribution, i.e., the real and imaginary parts of the r, z field components, is computed for reference throughout the whole domain by using 2–D FEM. Third–order triangles are used for the FEM discretization to get a very accurate results for comparisons with 3–D CM. Similarly, the magnetic flux density is evaluated within the conductor only to assess the local accuracy. For the 3–D CM model, tetrahedral meshes with different mesh sizes h

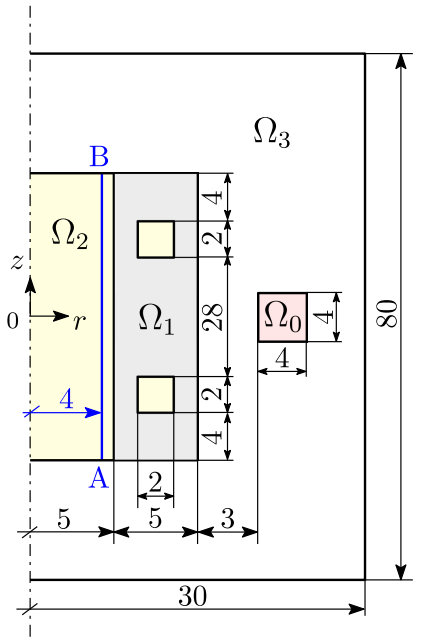

FIGURE 2. Axisymmetric inductor model: Ω_1 is the core domain (in gray, multiply connected), Ω_2 (in yellow) and Ω_3 (empty) are air domains, Ω_0 is the coil domain (in pink). All dimensions are in millimeters. The magnetic field is locally computed along the line A–B (in blue).

TABLE 1. Timings for the assembly and the solution of the final matrix system with TFQMR + SSOR (case 1, $\beta_1 = 3$).

h (mm)	# tets	# DOFs	CPU time (s) (assembly)	CPU time (s) (solution)
2.7	195 576	46 793	13.54	7.87
2.0	472 935	102 805	37.20	22.63
1.6	931 832	199 267	87.67	58.33
1.2	2 233 572	476 102	247.35	199.89
1.0	3 873 534	816 982	494.57	469.69

(reported in Table 1) are considered in order to check the convergence properties of the a–φ method. At this purpose the following relative errors (in the L^2–norm) for domains Ω and Ω_i are defined:

$$e_H = \frac{\|\mathbf{H}_h - \mathbf{H}\|_{L^2(\Omega)}}{\|\mathbf{H}\|_{L^2(\Omega)}}, \tag{81}$$

$$e_B = \frac{\|\mathbf{B}_h - \mathbf{B}\|_{L^2(\Omega_i)}}{\|\mathbf{B}\|_{L^2(\Omega_i)}}, \tag{82}$$

where $\mathbf{H}_h$, $\mathbf{B}_h$ are the approximated field distributions computed by the 3–D CM software and $\mathbf{H}$, $\mathbf{B}$ are the reference field distributions computed by third–order 2–D FEM.

Table 1 shows, for case 1 (multiply–connected Ω_i), the assembly time and the solution time needed for any mesh refinement. The assembly time encompasses the generation of both incidence and mass matrices, the generation of loop and source fields (by assuming an identity mass matrix), and

TABLE 2. Timings for the assembly and the solution of the final matrix system with TFQMR + SSOR (case 2, $\beta_1 = 0$).

h (mm)	# tets	# DOFs	CPU time (s) (assembly)	CPU time (s) (solution)
2.7	195 576	49 662	9.20	6.57
2.0	472 935	108 223	25.82	16.77
1.6	931 832	210 344	55.26	45.02
1.2	2 233 572	504 012	162.88	137.19
1.0	3 873 534	867 439	310.17	284.13

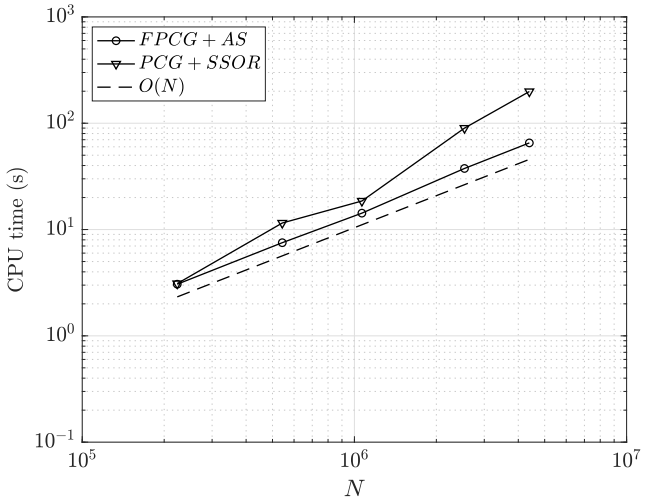

FIGURE 3. CPU time (s) vs. number of DOFs for PCG solver with SSOR preconditioner and for FPCG solver with the considered AS preconditioner.

the assembly of the final matrix system (67). In particular, loop fields are computed by using the algorithm presented in Section IV, with standard PCG + SSOR and AGMG iterative solvers (10^{-12} prescribed tolerance), and the final matrix system is solved with TFQMR + SSOR iterative solver (10^{-10} tolerance). The same tests are carried out also for case 2, with simply–connected Ω_i (Table 2). It can be observed that the number of DOFs is increased because more edge variables are used compared to case 1. On the other hand, timings for overall matrix system assembly and solution are lowered.

The performance of PCG solver with SSOR preconditioner is compared to that of FPCG solver with AS preconditioner by solving the equivalent curl-curl system (33), with identity mass matrix, for the same mesh refinements as above. Fig. 3 clearly shows that the FPCG with AS preconditioner attains optimal computational complexity. This proves that the algorithm for generating loop fields may be well suited for treating real–size eddy current problems with several millions of DOFs.

Fig. 4 and Fig. 5 show the errors (81) and (82), computed for the same mesh refinements as above. It can be observed that the a–φ method attains a first–order convergence rate in

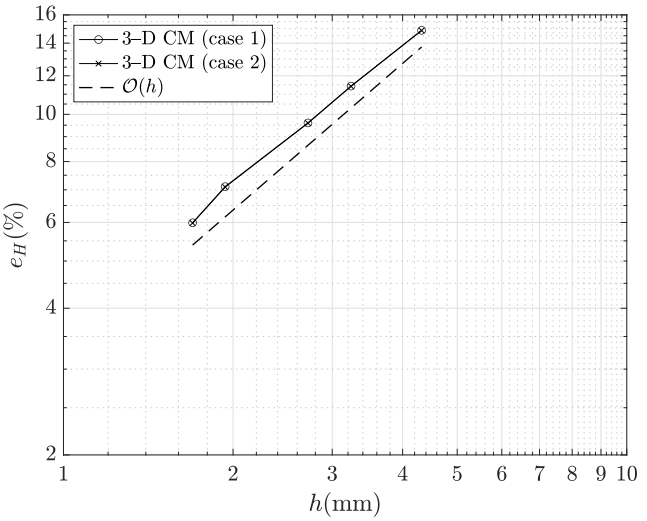

FIGURE 4. Discrepancy (L^2–norm) in Ω between the magnetic field of 3rd ord. 2-D FEM and 3–D CM. First–order convergence $\mathcal{O}(h)$ is in dashed line.

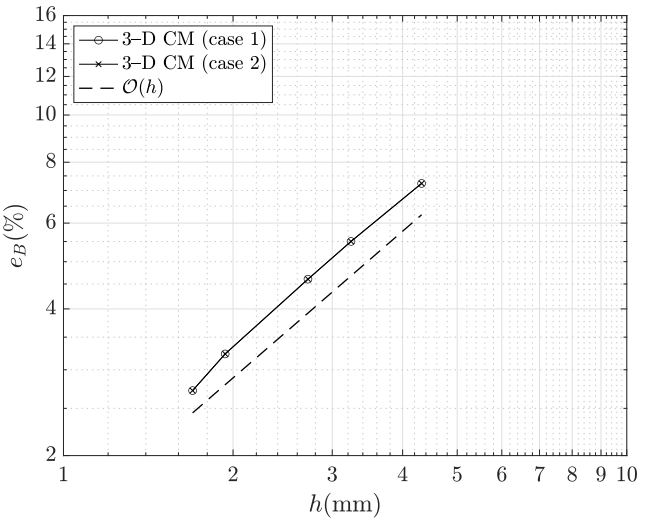

FIGURE 5. Discrepancy (L^2–norm) in Ω_i between the magnetic flux density of 3rd ord. 2-D FEM and 3–D CM. First–order convergence $\mathcal{O}(h)$ is in dashed line.

the L^2–norm, as already noted for the h–φ method. These tests are key in order to prove that a compatible coupling between electric and magnetic variables has been obtained by using the CM discretization scheme. In particular, Fig. 5 proves that a very good accuracy in the magnetic flux density reconstruction within the core is obtained by using the 3–D CM. Note that the same errors are attained for both cases 1 and 2, showing that the simplification of model topology does not affect the model accuracy.

The magnetic field is also locally computed in the air region, along the line A–B in Fig. 2, with coordinates $r = 4$ mm, $z = [-20, +20]$ mm. The z–axis field component (real and imaginary parts) is evaluated at 401 equally spaced points by using either 3–D CM or 2–D FEM. Although the coarsest mesh refinement is considered ($h = 2.7$ mm), numerical

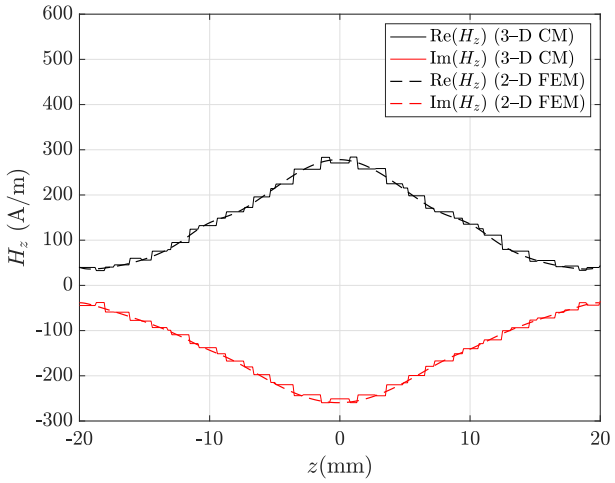

FIGURE 6. Real and imaginary parts of the z-axis magnetic field component along line A–B in Fig. 2 (case 1).

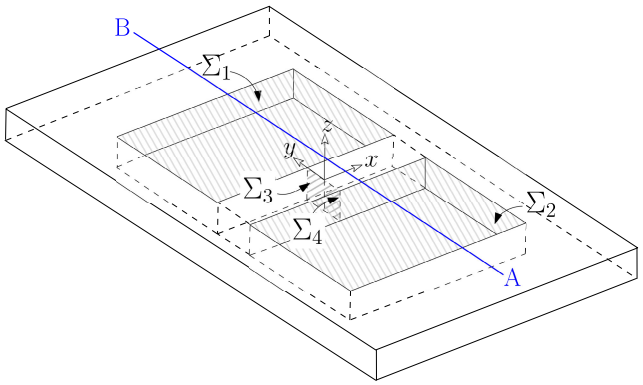

FIGURE 7. Line (in blue) and patches (in shaded gray) used for computing field quantities with 3–D CM and 3–D FEM.

results are in very good agreement for both the considered scenarios. For case 1, with $h = 2.7$ mm, the maximum discrepancies from 2–D FEM for the real and imaginary parts of H_z are 7.05% and 6.04%, respectively. For case 2, the discrepancies are 7.50% and 7.68%. This example shows that both modeling scenarios may lead to good accuracy also at local level, even with coarse meshes.

B. BATH PLATE BENCHMARK

The effectiveness of the a–φ method is evaluated on a classical benchmark for 3–D time–harmonic eddy–current problems, i.e, the so–called *Bath plate*. The benchmark is described in detail in [5] and it has already been used for validating the h–φ method. A conductive plate (32.78 MS/m conductivity, 1 relative permeability, 6.35 mm thick, 60 mm wide, 110 mm long) with two symmetric square holes (40 mm side) is excited by an AC current–driven coil (20 mm thick, 20 mm inner radius, 40 mm outer radius, 1240 A turn) by considering two different frequencies (50 Hz, 200 Hz). The whole model is embedded into a bounding box (200 mm side). Ω_i is represented by the conductor, whereas Ω_e is the air region (which includes the coil Ω_0). By a simple inspection of the model topology it can be observed that $\beta_1 = 2$, so that two loop fields are expected to be generated.

In order to assess the accuracy of a–φ method, its numerical results are compared with those from second–order 3–D FEM, based on the classical A, V–A formulation, taken as a reference. Note that, however, this formulation requires the introduction of a fake conductivity (0.1 S/m) in Ω_e for the stabilization of FEM solver, which is not required by a–φ method. Of course, this workaround introduces an additional approximation error for FEM.

For the CM, the whole domain is discretized into 213 640 tetrahedrons, where 154 635 elements are used for Ω_i and the rest for Ω_e. This discretization makes it possible to accurately resolve the skin effect within the plate at 200 Hz. The final matrix system of a–φ method (67) results in 117 496 DOFs (76 505 electric edge variables, 12 498 electric nodal potentials, 28 493 magnetic nodal potentials, 2 loop field coefficients). The system assembly procedure with the MATLAB code implementing the a–φ method is fast: 2.09 s CPU time are needed for building mass matrices, 1.90 s for incidence matrices, 2.32 s for source field, and 6.04 s for loops fields. The generation of source field includes the PCG + SSOR solution of the curl–curl system (38) of size 188 576). The generation of loop fields (i.e., the columns of $\mathbf{T}_{\Omega_e}$, with size 188 576), based on the algorithm in Section IV, includes the PCG + SSOR solution of the curl–curl matrix systems (33), with identity mass matrix, and AGMG solution of grad–grad matrix systems (35). The largest size of (33) is 188 575 and that of (35) is 28 492. Tolerances of both solvers used in the assembly are 10^{-12}. The final matrix system solution by TFQMR + SSOR iterative solver at 50 Hz takes 12.14 s CPU time (328 iterations to achieve the prescribed tolerance of 10^{-10}); at 200 Hz, 8.64 s (229 iterations) are required.

To get accurate reference values, the mesh used in the 2$^{\text{nd}}$ ord. FEM model is refined up to convergence. The final discretization results in 1 165 824 DOFs; FEM matrix system is solved by TFQMR + geometric multigrid solver with 10^{-10} tolerance in 161 s. To verify the accuracy of a–φ method, the z–component of the magnetic flux density (real and imaginary parts) is computed in 401 equally spaced points along the line A–B in Fig. 7, which is located 0.5 mm above the plate and is 110 mm long. The maximum discrepancies from 2$^{\text{nd}}$ ord. FEM are: 2.81% (real part) and 5.32% (imaginary part), at 50 Hz; 3.50% (real part) and 4.31% (imaginary part), at 200 Hz. These results show that even a first–order method such as CM can provide very good accuracy with a reasonable number of DOFs, when realistic engineering problems are analyzed.

As a comparison, a MATLAB implementation of the standard A, V–A formulation using first-order 3-D FEM is taken into account. The implementation is based on edge and face Whitney elements for building mass matrices, as described in [36]. The final matrix system structure is described e.g. in [37], and is solved by TFQMR + SSOR iterative solver. This formulation requires a careful treatment of the RHS

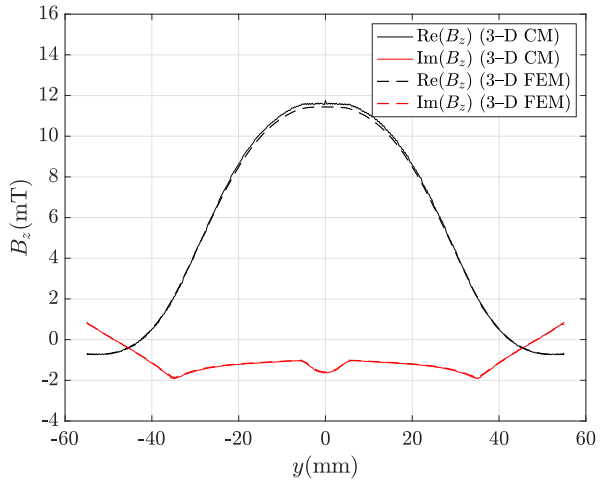

FIGURE 8. Real and imaginary parts of the z-axis magnetic flux density component at 50 Hz along line A–B; 3-D CM plot is in straight line, 3-D FEM plot is in dashed line).

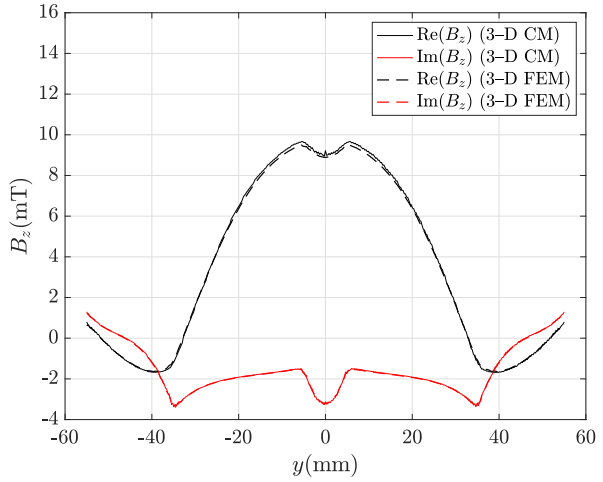

FIGURE 9. Real and imaginary parts of the z-axis magnetic flux density component at 200 Hz along line A–B; 3-D CM plot is in straight line, 3-D FEM plot is in dashed line).

to attain a good convergence behavior. The numerical strategy proposed by Ren is here adopted (see, in particular, (9) and (11) in [35]). With the same mesh as above, the final matrix system of the A, V–A method consists in 262 576 DOFs (250 078 electric edge variables, 12 498 electric nodal potentials), which is more than twice with respect to a–φ method. The CPU time for the assembly of A, V–A matrix system is 16.31 s and is larger than that of a–φ method, even though loop field generation is required in the second case. The solution time is almost twice as large as that of the a–φ method: the iterative solver attain the prescribed tolerance of 10^{-10} in 23.31 s, with 310 iterations, at 50 Hz, and 19.70 s, with 261 iterations, at 200 Hz. The accuracy of a–φ method is comparable to that of A, V–A method, with about half the DOFs of the latter. Discrepancies from 2$^{\text{nd}}$ order FEM are: 2.45% (real part), 5.78% (imaginary part) at 50 Hz; 2.88% (real part) and 6.75% (imaginary part), at 200 Hz.

TABLE 3. CPU time comparison of a–φ method with classical 1$^{\text{st}}$ ord. FEM (A, V–A method) and CM (h–φ method).

		# DOFs	Assembly (s)	Solution (s)	Total (s)
50 Hz	a–φ	117 498	14.02	12.14	26.16
	A, V–A	262 576	16.31	23.31	39.62
	h–φ	89 997	12.16	27.74	39.90
200 Hz	a–φ	117 498	13.20	8.58	21.78
	A, V–A	262 576	16.94	19.70	36.64
	h–φ	89 997	11.99	18.17	30.16

TABLE 4. Real and imaginary parts of magnetic flux (μ Wb) computed through surfaces Σ_1, Σ_2.

		$Re(b_{\Sigma_1})$	$Im(b_{\Sigma_1})$	$Re(b_{\Sigma_2})$	$Im(b_{\Sigma_2})$
50 Hz	CM	8.15	−1.91	7.99	−1.87
	FEM	7.84	−1.89	7.84	−1.89
200 Hz	CM	4.81	−3.09	4.71	−2.97
	FEM	4.49	−3.10	4.49	−3.10

For the sake of completeness the same simulation is run with the h–φ method, proposed by the authors in [5]. The final matrix system of the h–φ method consists in 89 997 DOFs (61 502 interior magnetic edge variables, 28493 magnetic nodal potentials, and 2 loop field coefficients), which are less than those of the a–φ method. The h–φ method requires, however, a more complex solution procedure: Lagrange multipliers are introduced to couple interior and exterior regions, and then are eliminated before solving. The system assembly requires 12.16 s CPU time, including the generation of loop fields with the algorithm described in [5], based on the LSMR iterative solver instead of PCG. Again the solution time with TFQMR + SSOR is more than twice with respect to a–φ method: 27.74 s at 50 Hz, with 1253 iterations, 18.17 s at 200Hz, with 808 iterations, to achieve 10^{-10} prescribed tolerance. Discrepancies from 2$^{\text{nd}}$ order FEM are close to those of a–φ method: 2.76% (real part), 5.06% (imaginary part) at 50 Hz; 3.72% (real part) and 5.82% (imaginary part), at 200 Hz.

Table 3 summarizes CPU times of assembly and solution obtained with the previous methods using the same discretization (213 640 tets, as described above). These show that a–φ method provides the best numerical performance.

The global quantities to be determined according to the Bath Plate benchmark are magnetic fluxes through patches Σ_1, Σ_2 and eddy currents through Σ_3, Σ_4 in Fig. 7. The real and imaginary parts of magnetic fluxes (Table 4) and eddy currents (Table 5), computed by 3–D CM and 3–D FEM at 50 Hz and 200 Hz are in good agreement. It can be observed

TABLE 5. Real and imaginary parts of eddy current (A) computed through surfaces Σ_3, Σ_4.

		$Re(I_{\Sigma_3})$	$Im(I_{\Sigma_3})$	$Re(I_{\Sigma_4})$	$Im(I_{\Sigma_4})$
50 Hz	CM	1.44	7.83	−1.42	−7.72
	FEM	1.37	7.54	−1.37	−7.54
200 Hz	CM	11.34	22.07	−11.14	−21.79
	FEM	10.88	21.34	−10.88	−21.34

that theoretical relationships $b_{\Sigma_1} = b_{\Sigma_2}$, $I_{\Sigma_3} = -I_{\Sigma_4}$, due to the model symmetry, are also fulfilled with good accuracy.

VII. CONCLUSION

A novel a–φ formulation, which combines the advantages of classical A, V–A and T–Ω formulations, has been proposed. The CM discretization scheme, based on pair of dual cells complexes, allows for consistently coupling electric and magnetic variables at the interface. Number of DOFs is almost halved with respect to an edge–based formulation like A, V–A, even though numerical results show that the same level of accuracy is obtained. The topological basis needed for the introduction of scalar potential is generated without need of thick cuts and with negligible computing time with respect to the overall assembly process. The assembly time of the a–φ method is smaller than the A, V–A method and comparable to the h–φ method. Lastly it has been proven by numerical experiments that accuracy remains unaltered if the model topology is simplified by extending the interior region with part of the insulating domain. Proposed algorithms for finding source and loop fields allow iterative solvers with optimal complexity to be adopted. From numerical experiments, first–order convergence for a–φ formulation has been proven on test case with complex topology. Moreover, computational requirements are limited even if real–size eddy–current problems are considered. Comparisons show that the a–φ method provides better performance than other existing methods such as A, V–A and h–φ.

REFERENCES

[1] O. Bíró, "Edge element formulations of eddy current problems," *Comput. Methods Appl. Mech. Eng.*, vol. 169, nos. 3–4, pp. 391–405, 1999.

[2] Z. Ren, "T-Ω formulation for eddy-current problems in multiply connected regions," *IEEE Trans. Magn.*, vol. 38, no. 2, pp. 557–560, Mar. 2002.

[3] M. Pellikka, S. Suuriniemi, L. Kettunen, and C. Geuzaine, "Homology and cohomology computation in finite element modeling," *SIAM J. Sci. Comput.*, vol. 35, no. 5, pp. B1195–B1214, Jan. 2013.

[4] S. Peltier, S. Alayrangues, L. Fuchs, and J.-O. Lachaud, "Computation of homology groups and generators," *Comput. Graph.*, vol. 30, no. 1, pp. 62–69, Feb. 2006.

[5] F. Moro, J. Smajic, and L. Codecasa, "A novel h–φ approach for solving eddy–current problems in multiply connected regions," *IEEE Access*, vol. 8, pp. 170659–170671, 2020.

[6] C. Emson and J. Simkin, "An optimal method for 3-D eddy currents," *IEEE Trans. Magn.*, vol. MAG-19, no. 6, pp. 2450–2452, Nov. 1983.

[7] R. Pillsbury, "A three dimensional eddy current formulation using two potentials: The magnetic vector potential and total magnetic scalar potential," *IEEE Trans. Magn.*, vol. MAG-19, no. 6, pp. 2284–2287, Nov. 1983.

[8] S. Polak, A. Wachters, and J. van Welij, "A new 3-D eddy current model," *IEEE Trans. Magn.*, vol. MAG-19, no. 6, pp. 2447–2449, Nov. 1983.

[9] D. Rodger and J. Eastham, "A formulation for low frequency eddy current solutions," *IEEE Trans. Magn.*, vol. MAG-19, no. 6, pp. 2443–2446, Nov. 1983.

[10] D. Rodger and J. Eastham, "Multiply connected regions in the A–ψ three-dimensional eddy-current formualtion," *IEE Proc. A Physical Sci., Meas. Instrum., Manage. Educ., Rev.*, vol. 134, pp. 58–66, Jan. 1987.

[11] A. Kameari, "Three-dimensional eddy current calculation using finite element method with AV in conductor and Omega in vacuum," *IEEE Trans. Magn.*, vol. MAG-24, no. 1, pp. 118–121, Jan. 1988.

[12] P. J. Leonard and D. Rodger, "Finite element scheme for transient 3D eddy currents," *IEEE Trans. Magn.*, vol. MAG-24, no. 1, pp. 90–93, Jan. 1988.

[13] O. Biro, K. Preis, and W. Renhart, "Finite element analysis of 3D multiply connected eddy current problems," *IEEE Trans. Magn.*, vol. 25, no. 5, pp. 4009–4011, Sep. 1989.

[14] P. J. Leonard and D. Rodger, "Comparison of methods for modelling jumps in conductivity using magnetic vector potential based formulations," *IEEE Trans. Magn.*, vol. 33, no. 2, pp. 1295–1298, Mar. 1997.

[15] A. Kameari, "Three dimensional eddy current calculation using edge elements for magnetic vector potential," in *Applied Electromagnetics in Materials*, K. Miya, Ed. Oxford, U.K.: Pergamon, 1989, pp. 225–236.

[16] A. Bossavit, "Two dual formulations of the 3-D eddy-currents problem," *Int. J. Comput. Math. Electr. Electron. Eng.*, vol. 4, no. 2, pp. 103–116, Feb. 1985.

[17] P. Lee, "A Lagrange multiplier method for the interface equations from electromagnetic applications," *SIAM J. Numer. Anal.*, vol. 30, no. 2, pp. 478–506, Apr. 1993.

[18] Z. Ren, C. Li, and A. Razek, "Hybrid FEM-BIM formulation using electric and magnetic variables," *IEEE Trans. Magn.*, vol. 28, no. 2, pp. 1647–1650, Mar. 1992.

[19] A. A. Rodríguez, R. Hiptmair, and A. Valli, "A hybrid formulation of eddy current problems," *Numer. Methods Partial Differ. Equ.*, vol. 21, no. 4, pp. 742–763, 2005.

[20] F. Moro and L. Codecasa, "A 3-D hybrid cell boundary element method for time-harmonic eddy current problems on multiply connected domains," *IEEE Trans. Magn.*, vol. 55, no. 3, pp. 1–11, Mar. 2019.

[21] F. Moro and L. Codecasa, "Coupling the cell method with the boundary element method in static and Quasi–Static electromagnetic problems," *Mathematics*, vol. 9, no. 12, p. 1426, Jun. 2021.

[22] E. Tonti, *The Mathematical Structure of Classical and Relativistic Physics: A General Classification Diagram*. Basel, Switzerland: Birkhäuser, 2013.

[23] A. A. Rodríguez, E. Bertolazzi, R. Ghiloni, and A. Valli, "Construction of a finite element basis of the first de rham cohomology group and numerical solution of 3D magnetostatic problems," *SIAM J. Numer. Anal.*, vol. 51, no. 4, pp. 2380–2402, Jan. 2013.

[24] R. Hiptmair and J. Ostrowski, "Coupled boundary-element scheme for eddy-current computation," *J. Eng. Math.*, vol. 51, no. 3, pp. 231–250, Mar. 2005.

[25] D. Arnold, *Finite Element Exterior Calculus*. Philadelphia, PA, USA: Society for Industrial and Applied Mathematics, 2018.

[26] L. Codecasa, "Refoundation of the cell method using augmented dual grids," *IEEE Trans. Magn.*, vol. 50, no. 2, pp. 497–500, Feb. 2014.

[27] E. Tonti, "Why starting from differential equations for computational physics?" *J. Comput. Phys.*, vol. 257, pp. 1260–1290, Jan. 2014.

[28] L. Codecasa and F. Trevisan, "Piecewise uniform bases and energetic approach for discrete constitutive matrices in electromagnetic problems," *Int. J. Numer. Methods Eng.*, vol. 65, no. 4, pp. 548–565, 2006.

[29] R. Hiptmair and J. Xu, "Auxiliary space preconditioning for edge elements," *IEEE Trans. Magn.*, vol. 44, no. 6, pp. 938–941, Jun. 2008.

[30] T. Kolev and P. Vassilevski, "Some experience with a H^1–based auxiliary space AMG for H(curl) problems," LLNL, Livermore, CA, USA, Tech. Rep. UCRL-TR-221841, 2006.

[31] A. Napov. *AGMG_CC: AGgregation-Based Algebraic MultiGrid Preconditioners for Curl-Curl Discretization*. Accessed: Oct. 19, 2021. [Online]. Available: http://metronu.ulb.ac.be/AGMG_CC

[32] Y. Notay, "Flexible conjugate gradients," *SIAM J. Scientific Comput.*, vol. 22, no. 4, pp. 1444–1460, Jan. 2000.

[33] E. F. Kaasschieter, "Preconditioned conjugate gradients for solving singular systems," *J. Comput. Appl. Math.*, vol. 24, nos. 1–2, pp. 265–275, Nov. 1988.

[34] A. Napov and Y. Notay, "An algebraic multigrid method with guaranteed convergence rate," *SIAM J. Sci. Comput.*, vol. 34, no. 2, pp. A1079–A1109, Jan. 2012.

[35] Z. Ren, "Influence of the RHS on the convergence behaviour of the curl-curl equation," *IEEE Trans. Magn.*, vol. 32, no. 3, pp. 655–658, May 1996.
[36] A. Bossavit, *Computational Electromagnetism: Variational Formulations, Complementarity, Edge Elements*. New York, NY, USA: Academic, 1998.
[37] H. Igarashi and T. Honma, "On convergence of ICCG applied to finite-element equation for quasi-static fields," *IEEE Trans. Magn.*, vol. 38, no. 2, pp. 565–568, Mar. 2002.

FEDERICO MORO (Member, IEEE) received the Laurea degree in electrical engineering, the Ph.D. degree in bioelectromagnetic and electromagnetic compatibility, and the B.S. degree in mathematics from the University of Padova, Italy, in 2003, 2007, and 2012, respectively. He was a Visiting Student at the Department of Physics, Swansea University, Wales, U.K., in 2005, and a Visiting Professor at the G2elab, Grenoble, France, in 2020. From 2007 to 2010, he was a Research Associate at the Department of Electrical Engineering, University of Padova. From 2010 to 2020, he was an Assistant Professor of electrical engineering at the Department of Industrial Engineering, University of Padova, where he has been working as an Associate Professor of electrical engineering, since 2020. He is the author of more than 100 articles in peer-reviewed international journals and conference proceedings. His research interests include numerical methods for computing electromagnetic problems and the numerical modeling of multiphysics and multiscale problems. He was awarded the Best Oral Presentation at UPEC 2006 and the Best Paper at ASME IDETC/CIE 2017 Conference and Electrimacs 2019 Conference. He received the National Scientific Qualification as a Full Professor (09/E1-Elettrotecnica), in 2021.

ARTEM NAPOV received the Ph.D. degree in engineering from the Université libre de Bruxelles (ULB), in 2010. From 2010 to 2012, he was a Postdoctoral Fellow at the Computational Science Division, Lawrence Berkeley National Laboratory. Since 2012, he has been working at École poytechnique de Bruxelles (ULB), as an Assistant Professor, where he has been an Associate Professor, since 2017. His research interest includes numerical methods for the solution of large sparse linear systems of equations arising from PDE discretizations.

LORENZO CODECASA (Member, IEEE) received the Ph.D. degree in electronic engineering from the Politecnico di Milano, in 2001. From 2002 to 2010, he worked as an Assistant Professor of electrical engineering at the Department of Electronics, Information, and Bioengineering, Politecnico di Milano, where he has been an Associate Professor of electrical engineering, since 2010. His main research contributions are in the theoretical analysis and in the computational investigation of electric circuits and electromagnetic fields. In his research on heat transfer and thermal management of electronic components, he has introduced original industrial-strength approaches to the extraction of compact thermal models, currently available in market leading commercial software. In his research areas, he has authored or coauthored over 200 papers in refereed international journals and conference proceedings. For these activities, he received the Harvey Rosten Award for Excellence, in 2016. He has also been serving as the Chair of the conference THERMal INvestigation of Integrated Circuits (THERMINIC). He has been serving as an Associate Editor for the IEEE TRANSACTIONS OF COMPONENTS, PACKAGING AND MANUFACTURING TECHNOLOGY.